



International Journal of Multidisciplinary Research in Science, Engineering and Technology

(A Monthly, Peer Reviewed, Refereed, Scholarly Indexed, Open Access Journal)



Impact Factor: 8.206

Volume 8, Issue 3, March 2025



International Journal of Multidisciplinary Research in Science, Engineering and Technology (IJMRSSET)

(A Monthly, Peer Reviewed, Refereed, Scholarly Indexed, Open Access Journal)

A Dynamic Hybrid Beamforming Approach for 5G-MIMO mmWave Wireless Cellular Networks

Dr. G. Naveen Kumar¹, K.Koushik², M.Tarakeswararao³, M.Venkata Kamal⁴, K.Hemanth⁵

Professor, Department of ECE, Vasireddy Venkatadri Institute of Technology, Nambur, Guntur, A.P., India¹

Undergraduate students, Department of ECE, Vasireddy Venkatadri Institute of Technology, Nambur, Guntur,
A.P., India²⁻⁵

ABSTRACT: Minimizing hardware complexity plays a crucial role in the design and deployment of next-generation broadband wireless networks. This study aims to assess the performance of an adaptive hybrid analog-digital beamforming approach within fifth-generation (5G) massive multiple-input multiple-output (MIMO) millimeter-wave (mmWave) wireless cellular environments. In this framework, beams are dynamically generated based on traffic demands through an on-off analog activation of radiating elements within each vertical antenna array. This mechanism enables the efficient delivery of high-data-rate services to active users without relying on expensive or mechanically complex steering antenna systems. Each vertical array, functioning as a radiating element within a circular array configuration, is assigned a dedicated radio frequency (RF) chain, forming the digital component of the system.

To evaluate the effectiveness of this approach, extensive Monte Carlo simulations were conducted for various MIMO configurations using a system-level simulator integrated with the latest 5G-3GPP channel model. The results demonstrate that the adaptive beamforming technique enhances key performance indicators (KPIs) such as total downlink transmission power and blocking probability. Specifically, in a MIMO configuration featuring 15 vertical antenna arrays and 10 radiating elements per array, the proposed adaptive algorithm significantly reduces the number of active radiating antenna elements compared to a static beam grid, depending on the tolerable transmission overhead. Furthermore, when maintaining a fixed number of radiating elements, both the total downlink transmission power and blocking probability show a substantial reduction. Notably, all KPI measurements were derived from the deployment of this array configuration in complex cellular environments, consisting of two tiers of cells surrounding a central cell.

KEYWORDS: 5G, hybrid beamforming, massive MIMO, millimeter wave communications, system-level simulations.

I. INTRODUCTION

With the rapid deployment of fifth-generation (5G) broadband wireless cellular networks, delivering ultra-low latency and high-data-rate services to mobile users necessitates a comprehensive network redesign. To achieve this vision, several advanced technologies have been introduced, including millimeter wave (mmWave) transmission, non-orthogonal multiple access (NOMA), and massive multiple-input multiple-output (MIMO) architectures. In the case of MIMO, a large number of antenna arrays are integrated into base stations (BSs) within cellular networks to efficiently serve mobile stations (MSs) demanding high data rates. This is accomplished through the generation of highly directional beams, which help mitigate multiple access interference (MAI).

Looking beyond 5G, the emergence of sixth-generation (6G) technology aims to establish seamless connectivity for all devices, everywhere. To enable this transition, existing 5G infrastructure must be adapted to high-frequency devices that support multi-gigabit-per-second data speeds—20 Gbps for downlink and 10 Gbps for uplink—with latencies as low as 1 ms. These high-bandwidth applications will require ultra-compact communication devices, making the design and operation of mmWave antenna configurations in 5G crucial for advancing 6G technologies. The integration of mmWave antennas into cellular systems allows for the development of high-performance BSs with flexible geometries and cost-effective construction. Additionally, the compact size of mmWave antennas facilitates the deployment of numerous adaptable BS configurations, accommodating dynamic traffic demands and improving overall network throughput.



International Journal of Multidisciplinary Research in Science, Engineering and Technology (IJMRSET)

(A Monthly, Peer Reviewed, Refereed, Scholarly Indexed, Open Access Journal)

In conventional multi-user (MU) MIMO systems, fully digital (FD) precoding is commonly used to adjust the amplitude and phase of transmitted signals for optimal beamforming. However, in massive MIMO deployments, FD precoding presents substantial computational and hardware challenges, as the number of required radio frequency (RF) chains scales with the number of antennas. To address this issue, most research efforts focus on suboptimal beamforming techniques based on hybrid beamforming (HBF). The HBF architecture combines a digital precoder at the baseband level with an analog precoder in the RF domain, significantly reducing the number of required RF chains by leveraging the low-dimensional digital precoder. This paper evaluates the performance of a low-complexity HBF structure when deployed in massive MIMO mmWave multicellular environments.

II. ANTENNA DESIGN

The structure of the proposed adaptive beamformer is illustrated in Fig. 1. On the transmitter side, a baseband digital precoder (FBB) processes N_s data streams to generate N_s RF outputs at the base station (BS). Throughout this study, a diversity combining transmission mode is assumed, where $N_s = K_b N_s = K_b N_s = K_b$, representing the number of mobile stations (MSs) within the b th BS ($1 \leq b \leq B$). However, the proposed approach can be easily extended to accommodate spatial multiplexing transmission as well. The FBB matrix has dimensions $K_b \times v K_b \times v$, with each of the v RF chains connected to a subset of w transmitting antennas within a specific vertical array, as depicted in Fig. 1. Each transmitting antenna within an RF subset can be dynamically switched on or off based on channel state information (CSI) at the BS, enabling an adaptive beamforming mechanism. This on-off analog beamforming significantly reduces both hardware complexity and algorithmic overhead. While this structure aligns with a partially connected hybrid beamforming (PC-HBF) architecture, each v RF chain is dedicated to covering a distinct angular region, eliminating the need for interconnecting all RF chains with every transmitting antenna.

Each RF chain consists of a vertical array of w crossed dipole (CD) antennas designed to operate at the mmWave frequency of 28 GHz, as shown in Fig. 2. Additionally, the v RF chains are arranged in a circular array with equal spacing, determined by $a = 360^\circ / v = 360^\circ / v = 360^\circ / v$. Each CD antenna comprises two identical, orthogonally oriented ($\pm 45^\circ$) radiating half-wave dipoles, as illustrated in Fig. 3. The input voltage at the antenna port is set to 1V, with a phase difference of 0° between the dipoles, thereby establishing a dual-polarization (DP) antenna configuration. This configuration is achieved through the use of separate feeding ports, which play a crucial role in optimizing beamforming performance for 5G applications.

To further enhance gain in the horizontal plane, each vertical crossed dipole is spaced at $\lambda/2$ apart, where λ represents the carrier wavelength. For unidirectional DP radiation, all radiating elements are positioned above a perfect electric conductor (PEC) reflector at an approximate distance of $\lambda/4$, contributing to additional gain improvement. Finally, the width and spacing between the two radiating elements are on the order of $\lambda/100$, as depicted in the profile view of the CD antenna in Fig. 3.

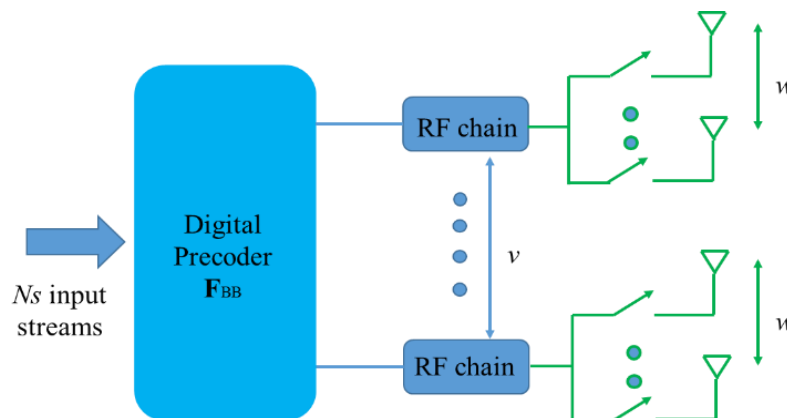
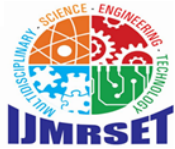


FIGURE 1. Proposed adaptive beamformer structure.



International Journal of Multidisciplinary Research in Science, Engineering and Technology (IJMRSET)

(A Monthly, Peer Reviewed, Refereed, Scholarly Indexed, Open Access Journal)

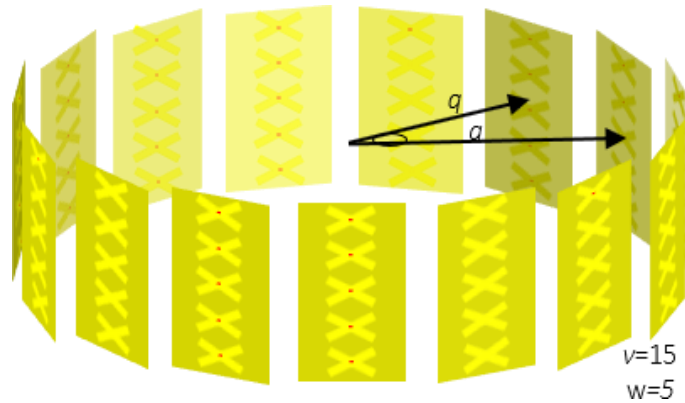


FIGURE 2. An example of circular array. This geometry consists of 15 RF chains and 75 ($v \times w$) crossed half-wave dipoles (150 radiating elements) uniformly distributed, $a=360/15=24^\circ$, with a ring radius q .

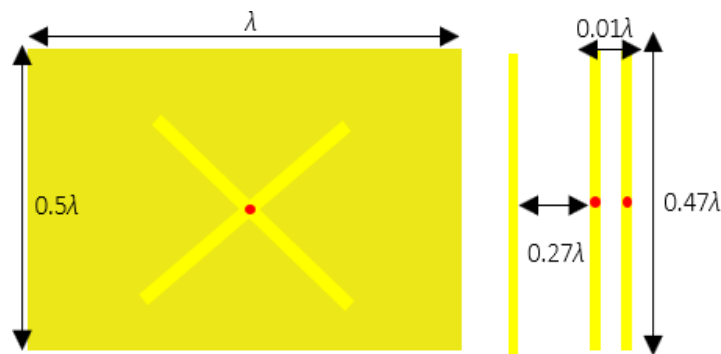


FIGURE 3. Geometry of the reflector using a crossed dipole as an exciter.

The electromagnetic analysis of the circular array depicted in Fig. 2 was conducted using the Method of Moments (MoM) [36]. In this analysis, each study is uniquely defined by the parameters www , qqq , vvv , and aaa . Notably, the simulations account for the significant mutual coupling effects among all radiating elements ($v \times w \times 2v \times w \times 2$). Accordingly, variations in both the radiation pattern and the input impedance of the array were incorporated into our 3D computational model .

The study presents two distinct sets of simulations. The first set follows a fixed grid of beams (FGoB) approach, where the array configuration remains constant, characterized by specific values of qqq , www , vvv , and aaa . Conversely, in the second set of simulations, qqq and vvv values remain unchanged, while aaa and www values are variable, resulting in different azimuth radiation patterns that define the beamforming technique .

In the FGoB simulations, four unique array geometries are examined, as shown in Fig. 4. The parameters for these configurations are set as $q=0.149\lambda$, $q=0.149\lambda$, with $a=120^\circ$ in Fig. 4(a,b), and $a=45^\circ$ in Fig. 4(c,d). Additionally, Fig. 4 illustrates the gain distribution on the azimuth plane, providing insight into the beam orientations. As expected, increasing the number of vertical arrays results in a greater number of generated beams. Similarly, a higher count of crossed dipoles (CDs) within each vertical array enhances the maximum gain (G_{max}) of the overall configuration.

The corresponding G_{max} values are displayed in the column of Fig. 4. Notably, the Half Power Beam Width (HPBW) for the configurations in Fig. 4(a-d) measures 70° , 69° , 21° , and 21° , respectively. In these cases, all radiating elements are equally excited. An alternative approach to improving energy efficiency and enhancing Quality of Service (QoS) for mobile stations (MSs) is adaptive beamforming. Unlike FGoB, adaptive beamforming does not



International Journal of Multidisciplinary Research in Science, Engineering and Technology (IJMRSET)

(A Monthly, Peer Reviewed, Refereed, Scholarly Indexed, Open Access Journal)

maintain a fixed number and position of active CDs. Instead, the number of beams and their orientations dynamically adjust based on the number and location of active MSs.

Certain circular array configurations with fixed values of v , q , and a but different w values can form beams with varying gains and orientations, as demonstrated in Fig. 5. A key characteristic of the configuration in Fig. 5 is the initial number of radiating elements (w_{0w_0}), which significantly influences the gain distribution across predefined angular directions. Specifically, Fig. 5(a) presents an array configuration with $w_0=4$, $v=15$, $q=2.94\lambda$, and $a=120^\circ$. Depending on the number and position of the MSs, the circular array configuration in Fig. 5 can either rotate its entire radiation pattern or shift individual beams by $\pm 24^\circ$ ($360/v$).

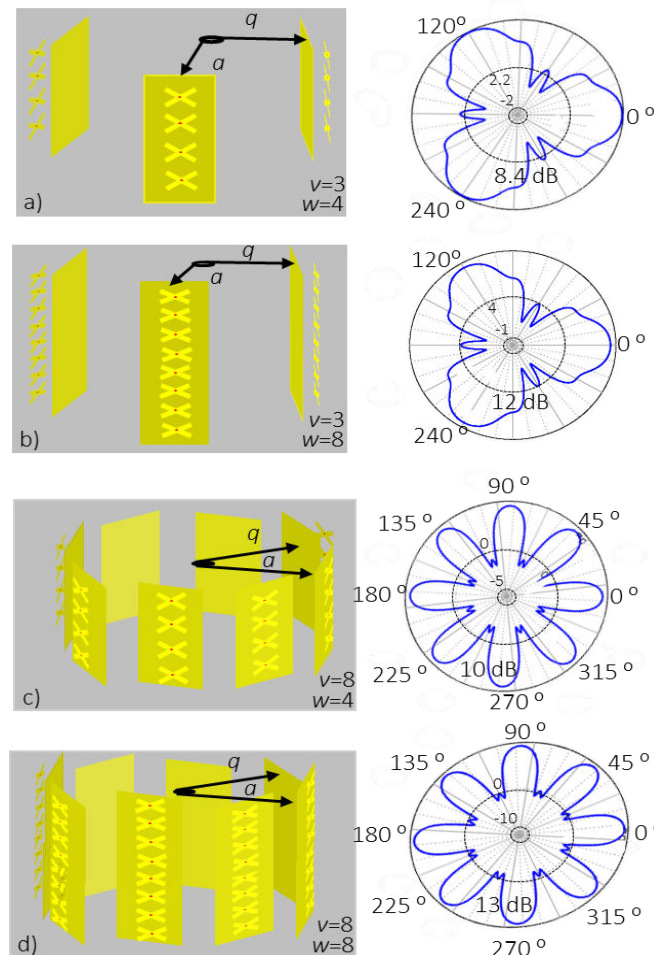
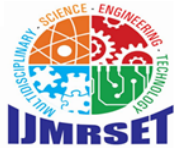


FIGURE 4. Circular array configuration and gain (dB) on the horizontal plane (azimuth) for certain parameters.

When the number of mobile stations (MSs) increases in a specific angular location, as illustrated in Fig. 5(c), the array configuration adapts by increasing the number of active radiating elements from $w_0=4$ to $w=5$ in the corresponding 24° sector, while maintaining $w_0=4$ in the remaining 120° and 240° sectors. The blue arrows in Fig. 5(a) indicate these dynamic activations of vertical arrays relative to their initial state. Notably, for $w_0=4$, the maximum gain (G_{max}) is 9 dB with a Half Power Beam Width (HPBW) of 58° . When w increases to 5, G_{max} rises to 10.4 dB, while HPBW expands to 70° .



International Journal of Multidisciplinary Research in Science, Engineering and Technology (IJMRSET)

(A Monthly, Peer Reviewed, Refereed, Scholarly Indexed, Open Access Journal)

A special case of adaptive beamforming is presented in Fig. 5(h), where $w_{ow} = 5$ is increased to $w = 5w = 5w = 5$ across the entire array configuration, reflecting a scenario where traffic demand rises uniformly across all predefined angular sectors. While w can theoretically take higher values, such as 10 or 15, this would significantly increase computational complexity and extend the duration of Method of Moments (MoM) simulations. Therefore, for the purpose of this study, the optimal maximum value of w is set to 5.

Ultimately, the array configuration, along with its corresponding horizontal plane beamwidths (as depicted in Fig. 5), presents a multifunctional, cost-effective, and low-complexity hardware solution. By selectively activating vertical arrays at specific angular positions without requiring a mechanical steering system, this approach greatly simplifies the design and deployment of next-generation broadband wireless networks.

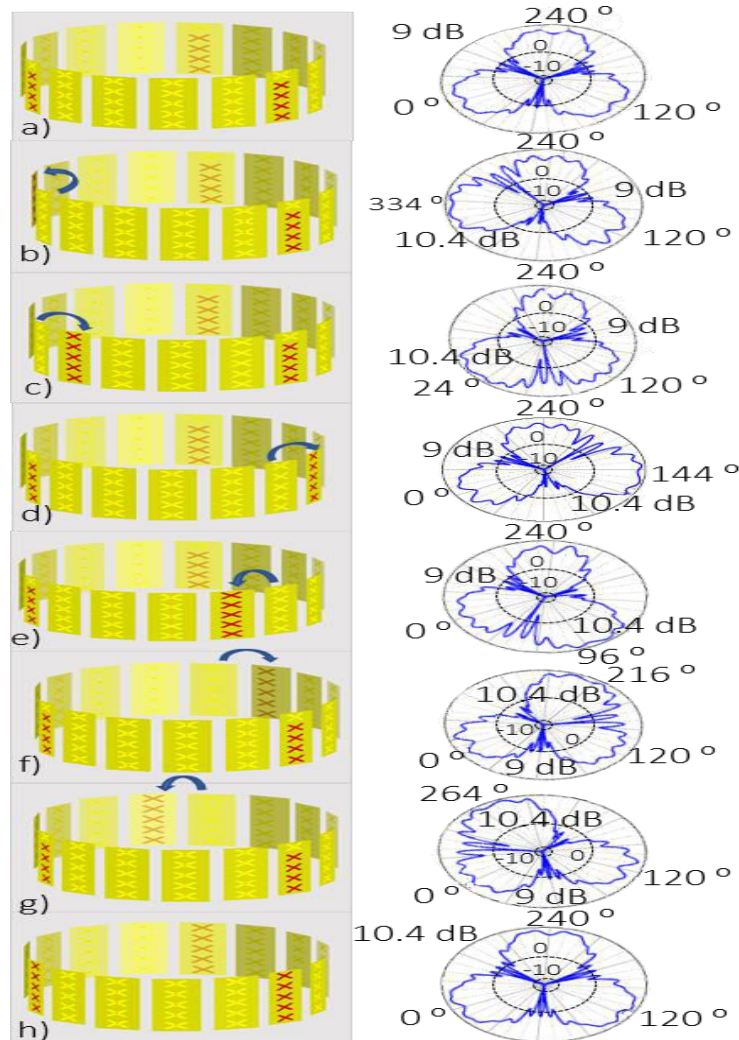


FIGURE 5. Different circular array configurations along with their corresponding horizontal plane beamwidths (azimuth) (the activated CDs are illustrated with red color and angle counting starts from the first activated array on the left, Fig. 5(a), for illustrating purposes).



International Journal of Multidisciplinary Research in Science, Engineering and Technology (IJMRSET)

(A Monthly, Peer Reviewed, Refereed, Scholarly Indexed, Open Access Journal)

III. RESULTS

A. FIXED GRID OF BEAMS PER BS

The first set of simulation results, corresponding to the fixed grid of beams (FGoB) approach, is presented in Figs. 6–8 for the antenna geometries outlined in Fig. 4. In all figures, cumulative distribution function (CDF) curves are plotted against each of the key performance indicators (KPIs) discussed in Section II.

Since adaptive modulation and coding per subcarrier is beyond the scope of this study, we assume a uniform transmission rate for all mobile stations (MSs), denoted as $R_k = RR_k = R$. This transmission rate can be achieved through an appropriate allocation of physical resource blocks (PRBs) and a suitable modulation order per PRB. In all simulation scenarios, each MS can be allocated either 5 or 15 PRBs, resulting in supported bit rates of 7.2 Mbps or 21.6 Mbps, respectively. These values are determined by the product of the assigned PRBs per MS, the number of subcarriers per PRB, the subcarrier spacing, and the bits transmitted per subcarrier, as defined by the modulation scheme (refer to Table I).

TABLE I
SIMULATION PARAMETERS

Parameter	Value/Assumption
Tiers of cells	2
Pathloss model	UMa
Carrier frequency (GHz)	28
Channel Bandwidth (MHz)	100
Subcarrier spacing (kHz)	60
Subcarriers per PRB	12
Cell radius (m)	500
Assigned PRBs per MS	5/15
Monte Carlo snapshots per scenario	10^4
Required E_b/N_0 (dB)	9.6 [43]
Maximum transmission power per BS/MS (W)	20/1
Considered antenna geometries at BSs ($v \times w$)	$3 \times 4, 3 \times 8, 8 \times 4, 8 \times 8, 15 \times 5$
Antenna elements per MS	2
Transmission mode	Diversity Combining

Additionally, the simulation considers wireless network deployments with two tiers of cells surrounding a central cell. A summary of all simulation parameters is provided in Table I, ensuring consistency with the majority of related studies in [2]. Throughout this subsection, the notation (v, w, R) is used in figure legends, where "active beams" refers to the number of generated beams per base station (BS), as all vertical arrays are activated.



International Journal of Multidisciplinary Research in Science, Engineering and Technology (IJMRSET)

(A Monthly, Peer Reviewed, Refereed, Scholarly Indexed, Open Access Journal)

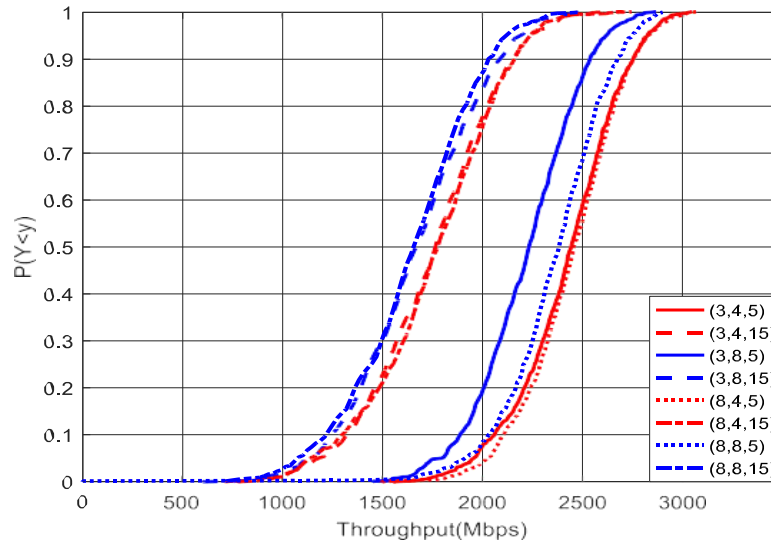


FIGURE 6. Total network throughput (Mbps).

As illustrated in Fig. 6, throughput is maximized when each mobile station (MS) is allocated 5 physical resource blocks (PRBs), with four radiating elements per vertical array and three or eight active beams per BS (represented by the group of two curves on the right side of Fig. 6). Notably, an increase to eight radiating elements per vertical array results in a decline in throughput. While a higher number of radiating elements enhances spatial directivity, it simultaneously reduces overall spatial coverage. In all cases, throughput decreases when 15 PRBs are assigned per MS, as expected, since high data rate services can only be provided to a limited number of active MSs. Similar to the case of 5 PRBs per MS, throughput is optimized when the number of crossed dipoles (CDs) per vertical array is limited.

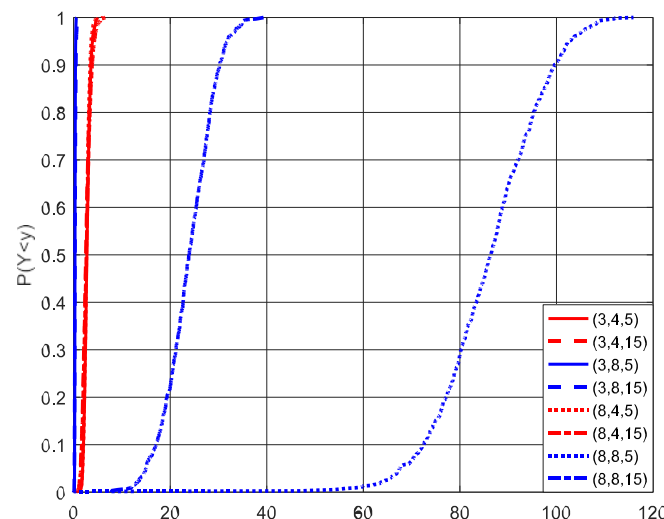


FIGURE 7. Total transmission power (W).



International Journal of Multidisciplinary Research in Science, Engineering and Technology (IJMRSET)

(A Monthly, Peer Reviewed, Refereed, Scholarly Indexed, Open Access Journal)

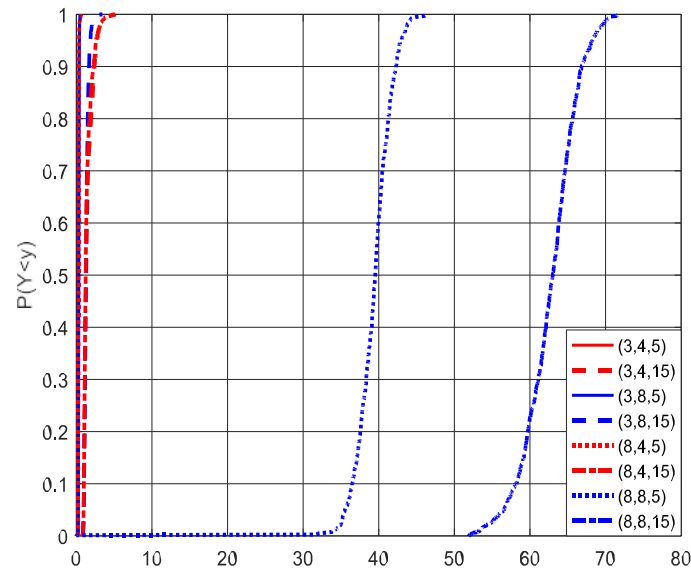


FIGURE 8. Blocking probability (%).

Fig. 7 presents the cumulative distribution function (CDF) curves for total downlink transmission power. Transmission power peaks when each MS is assigned five PRBs, with eight CDs per vertical array and eight active beams per BS. In this scenario, given that the median blocking probability (BP) reaches nearly 30% (as shown in Fig. 8), additional transmission power is required to compensate for reduced spatial coverage. Conversely, in configurations with four CDs per vertical array (5/15 PRBs per MS and three/eight active beams), both BP and total downlink transmission power are minimized.

From these observations, it is evident that the formation of highly directional beams in predefined angular locations can lead to an increase in downlink transmission power and a decline in BP due to reduced spatial coverage. To address this, the next subsection considers the antenna geometry from Fig. 5, where three active beams are generated per Monte Carlo (MC) snapshot based on the distribution of MSs. This ensures 360° spatial coverage, which depends on the orientation of the activated vertical arrays and the number of active CDs per vertical array. These parameters are dynamically adjusted according to traffic demands.

B. ADAPTIVE GRID OF BEAMS

In the second set of simulation results (Figs. 9-12), the proposed adaptive beamforming (AGoB) approach is analyzed. The antenna geometry from Fig. 5 is implemented in each active base station (BS), and its performance is compared against the fixed grid of beams (FGoB) scenario, where three beams per BS are generated at $\{0^\circ, 120^\circ, 240^\circ\}$. Additionally, Fig. 12 introduces a new key performance indicator (KPI): the total number of radiating elements per Monte Carlo (MC) simulation in both the AGoB and FGoB scenarios. In all figures, the notation (v, w, R) is used for the FGoB case (also referred to as FB), while (v, w, w_o, R) is used for the AGoB case (also referred to as AB). Throughout the analysis, unless stated otherwise, all KPIs are compared based on their mean values.

As shown in Fig. 9, there is no significant variation in throughput between the AGoB and FGoB cases for the considered MIMO configurations. However, Fig. 12 highlights a substantial reduction in the total number of radiating elements in the AGoB scenario. For instance, when each mobile station (MS) is allocated 5 physical resource blocks (PRBs) and $w_o = 3$ in the AGoB case, the mean total throughput remains at 2245 Mbps, similar to the FGoB case. However, only 190 radiating elements are activated in AGoB, compared to 285 in FGoB. This number increases to 230 when $w_o = 4$, but with a corresponding reduction in transmission power. Specifically, the mean transmission power values for $w_o = 3$ and $w_o = 4$ are 17 W and 10 W, respectively.

For the case of 15 PRBs per MS, the total network throughput is 1700 Mbps. The number of active radiating elements is now 182 (AGoB with $w_o = 3$), 223 (AGoB with $w_o = 4$), and 277 (FGoB). Corresponding transmission power



International Journal of Multidisciplinary Research in Science, Engineering and Technology (IJMRSET)

(A Monthly, Peer Reviewed, Refereed, Scholarly Indexed, Open Access Journal)

values are 9 W, 6 W, and 4.8 W, respectively. Furthermore, when $w_0 = 4$, blocking probability (BP) is reduced in comparison to the FGoB approach. For 5 PRBs per MS, BP values are 0.75% (FGoB) and 0.5% (AGoB), whereas for 15 PRBs per MS, they are 3.8% and 2.5%, respectively.

A key observation from these results is the trade-off between hardware complexity reduction (expressed via the reduced number of radiating elements) and total downlink transmission power. The FGoB scenario exhibits lower mean transmission power compared to AGoB. To address this, an additional MIMO configuration is evaluated where $w_0 = 5$. In this scenario, the number of active RF chains remains similar for both the fixed and adaptive beam cases. However, as illustrated in Fig. 10, overall transmission power in the AGoB scenario is lower at 6.3 W compared to 7 W in the FGoB case for 5 PRBs per MS. Similarly, for 15 PRBs per MS, the transmission power values are 4.2 W (AGoB) and 4.8 W (FGoB). The BP follows the same trend, reducing to 0.4% and 2.1% for 5 and 15 PRBs per MS, respectively, in the AGoB scenario.

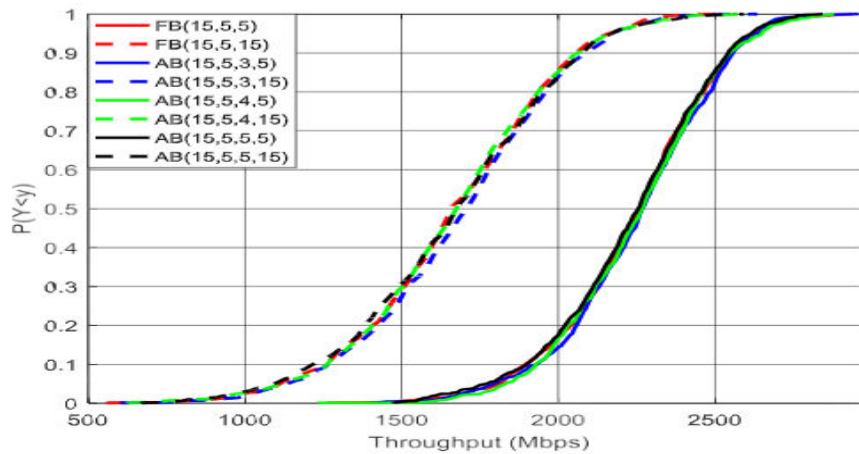


FIGURE 9. Total network throughput (Mbps)

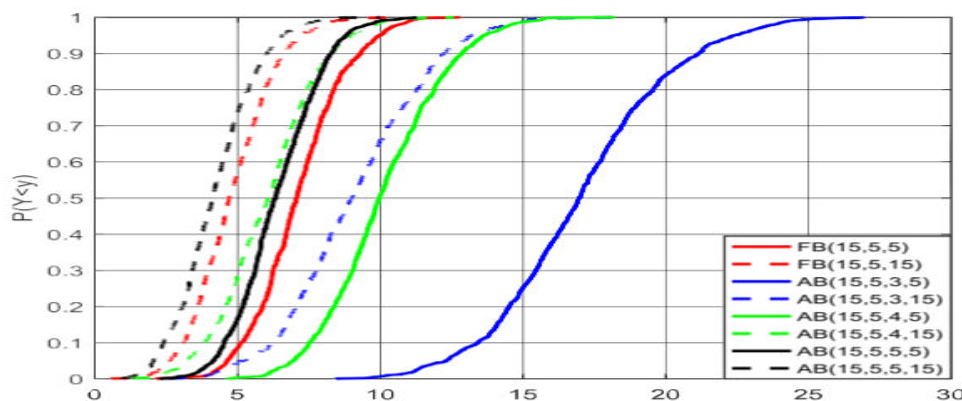


FIGURE 10. Total transmission power (W).



International Journal of Multidisciplinary Research in Science, Engineering and Technology (IJMRSET)

(A Monthly, Peer Reviewed, Refereed, Scholarly Indexed, Open Access Journal)

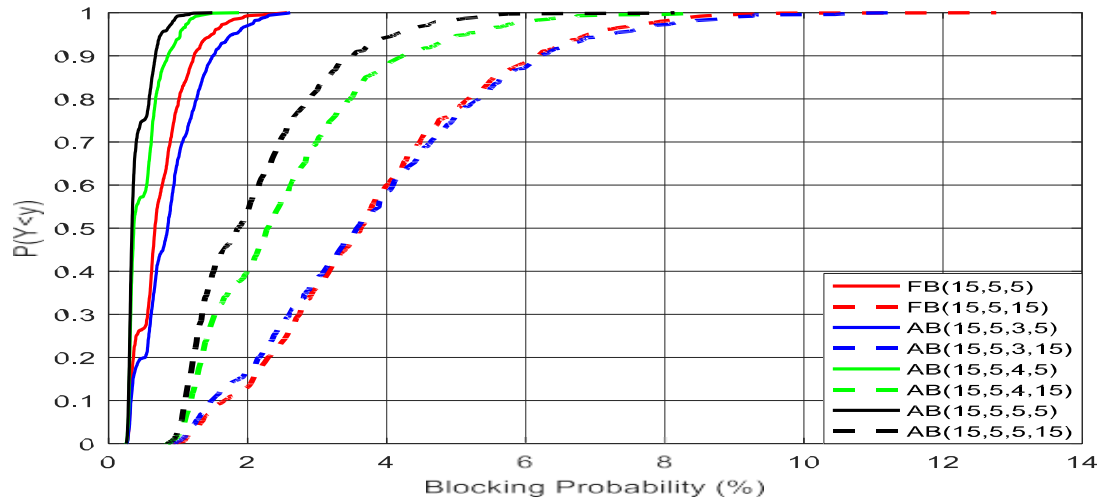


FIGURE 11. Blocking probability (%).

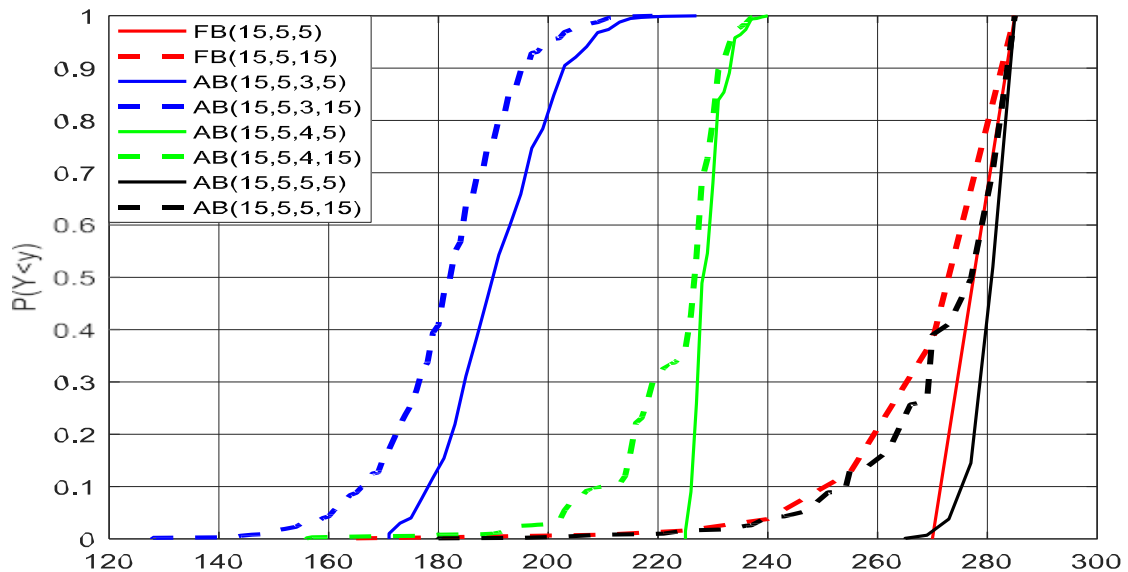


FIGURE 12. Active radiating elements.

IV.CONCLUSION

The performance of an adaptive hybrid beamforming approach in 5G mmWave cellular networks has been evaluated. In this approach, a separate RF chain is assigned to each vertical antenna array, with radiation pattern formation achieved by activating different sets of antenna elements. Each vertical array serves as a radiating element within a circular array configuration, ensuring broad 360° spatial coverage.

The results indicate that while reducing hardware complexity—expressed through a lower number of active radiating antenna elements—leads to increased transmission power, the proposed adaptive beamforming method enhances key performance indicators (KPIs). Specifically, it improves total downlink transmission power when all radiating elements per vertical antenna array are activated and reduces blocking probability.



International Journal of Multidisciplinary Research in Science, Engineering and Technology (IJMRSET)

(A Monthly, Peer Reviewed, Refereed, Scholarly Indexed, Open Access Journal)

It is important to note that the proposed adaptive beamforming scheme assumes perfect channel state information (CSI) at the base stations (BSs). However, this approach can be extended to scenarios where the analog stage employs codebook-based searching, eliminating the need for direct channel estimation in high-dimensional analog channels.

Future work will explore the application of this approach in more demanding traffic scenarios, such as user-specific directive beam formation, as well as in distributed MIMO architectures. The insights from this study can contribute to optimizing array configurations in terms of directivity and physical size, particularly through the use of chip-scale radiating elements. Additionally, investigating smart antennas and plasmonic nanoantennas at optical frequencies could pave the way for advanced 6G applications.

REFERENCES

- [1] Y. Xu, G. Gui, H. Gacanin and F. Adachi, "A survey on resource allocation for 5G heterogeneous networks: Current research, future trends, and challenges," *IEEE Commun. Surv. Tutor.*, vol. 23, no. 2, pp. 668-695, Secondquarter 2021.
- [2] P. K. Gkonis, P.K.; Trakadas and D. I. Kaklamani, "A comprehensive study on simulation techniques for 5G networks: State of the art, analysis and future challenges," *Electronics*, vol. 9, no. 3, DOI: 10.3390/electronics9030468.
- [3] A. N. Uwaechia and N. M. Mahyuddin, "A comprehensive survey on millimeter wave communications for fifth-generation wireless networks: Feasibility and challenges," *IEEE Access*, vol. 8, pp. 62367-62414, Mar. 2020.
- [4] B. Makki, K. Chitti, A. Behravan and M. -S. Alouini, "A survey of NOMA: Current status and open research challenges," *IEEE OJ-COMS*, vol. 1, pp. 179-189, Jan. 2020
- [5] A. Ghosh, A. Maeder, M. Baker and D. Chandramouli, "5G evolution: A view on 5G cellular technology beyond 3GPP release 15," *IEEE Access*, vol. 7, pp. 127639-127651, Sept. 2019.
- [6] M. Soleimani, R. C. Elliott, W. A. Krzymień, J. Melzer and P. Mousavi, "Hybrid beamforming for mmWave massive MIMO systems employing DFT-assisted user clustering," *IEEE Trans. on Veh. Tech.*, vol. 69, no. 10, pp. 11646-11658, Oct. 2020.
- [7] M. S. Aljumaily and H. Li, "Machine learning aided hybrid beamforming in massive-MIMO millimeter wave systems," *IEEE International Symposium on Dynamic Spectrum Access Networks (DySPAN)*, Newark, NJ, USA, 11-14 Nov. 2019, pp. 1-6, DOI: 10.1109/DySPAN.2019.8935814.
- [8] C. Balanis, *Antenna Theory: Analysis and Design*, Willey, 2016.
- [9] K. Mahmoud, M. El-Adawy, S. Ibrahim, R. Bansal and
- [10] S. Zainud-Deen, "A comparison between circular and hexagonal array geometries for smart antenna systems



INTERNATIONAL
STANDARD
SERIAL
NUMBER
INDIA



INTERNATIONAL JOURNAL OF MULTIDISCIPLINARY RESEARCH IN SCIENCE, ENGINEERING AND TECHNOLOGY

| Mobile No: +91-6381907438 | Whatsapp: +91-6381907438 | ijmrset@gmail.com |

www.ijmrset.com